Uniform Colloidal Spheres for $(Y_{1-x}Gd_x)_2O_3$ ($x = 0$–1): Formation Mechanism, Compositional Impacts, and Physicochemical Properties of the Oxides

Ji-Guang Li,*[,†,‡] Xiaodong Li,[‡] Xudong Sun,[‡] Takayasu Ikegami,[†] and Takamasa Ishigaki[†]

Nano Ceramics Center, National Institute for Materials Science, Namiki 1-1, Tsukuba, Ibaraki 305-0044, Japan, and Key Laboratory for Anisotropy and Texture of Materials (Ministry of Education), School of Materials and Metallurgy, Northeastern University, Shenyang 110004, China

Received November 22, 2007. Revised Manuscript Received January 7, 2008

Uniform spheres of $(Y_{1-x}Gd_x)_2O_3$ ($x = 0$–1) are valuable for applications in phosphors, in optical ceramics fabrication, and in combinatorial synthesis. We made in this work such particles by thermal decomposition of precursors synthesized via homogeneous precipitation. Growth kinetics and composition evolution of the precursor spheres were investigated in detail, and it was identified for the first time that (1) differential nucleation occurs with regard to Y and Gd, and as a result concentration gradients exist within each precursor particle of the mixed Y/Gd system (more Gd and less Y from particle surface to the core), (2) average particle size of the colloidal sphere is inversely proportional to nucleation density and is significantly affected by the Gd content, (3) growth of the colloidal spheres is diffusion controlled and follows the cubic-root law, and (4) the dried precursor spheres directly convert to cubic-structured $(Y_{1-x}Gd_x)_2O_3$ ($x = 0$–1) oxides at 1000 °C while largely retaining their morphologies. The resultant oxides exhibit linearly increased lattice parameters and linearly decreased bandgaps (from 5.57 eV for Y_2O_3 to 5.20 eV for Gd_2O_3) with increased Gd addition. The findings of this work may have wide implications to other mixed materials systems.

1. Introduction

Monodispersed colloidal spheres of uniform size and shape play important roles in understanding the optical, magnetic, electronic, and electrokinetic properties of the materials. When used as stable suspensions, the colloidal spheres have been finding increased applications in fields such as drug delivery, biolabeling, and combinatorial synthesis. More importantly, the monodispersed colloidal particles may be assembled into arrays or domains that allow one to obtain functionalities not only from the constituent materials but also from the long-range periodic structures.[1–8] A handful of chemical strategies[9–19] are now available to synthesize monodispersed colloidal spheres, and the most matured ones seem to be the homogeneous precipitation technique for inorganic particles[9–20] and the emulsion polymerization technique for polymer latexes.[21,22] With the urea-based homogeneous precipitation (UBHP) technique, a variety of inorganic particles with uniform size and well-defined morphologies have been synthesized by taking advantages of the slow decomposition of urea at elevated temperatures (≥83 °C), which serves as a reservoir for precipitating anions.[9–14] The in situ decomposition of urea releases precipitating ligands (mainly OH^- and CO_3^{2-})[23] slowly and homogeneously into the reaction system, avoiding localized distribution of the reactants and thus making it possible to exercise control over nucleation and growth. The formation of monodispersed colloidal particles has largely been explained by the LaMer model,[12,24] which emphasizes a single burst nucleation followed by uniform growth, that is, a strict separation of the nucleation and growth stages. It should be noted that the LaMer model may not be valid in some cases, and a number of recent studies[12,25–29] suggested that several

* Corresponding author. Tel.: +81-29-860-4394. Fax: +81-29-860-4701. E-mail: li.jiguang@nims.go.jp.
† National Institute for Materials Science.
‡ Northeastern University.

(1) Xia, Y. N.; Gates, B.; Li, Z.-Y. *Adv. Mater.* **2001**, *13*, 409.
(2) Pieranski, P. *Contemp. Phys.* **1983**, *24*, 25.
(3) Van Megan, W.; Snook, I. *Adv. Colloid Interface Sci.* **1984**, *21*, 119.
(4) Gast, A. P.; Russel, W. B. *Phys. Today* **1998**, (December), 24.
(5) Grier, D. G., Ed. From Dynamics to Devices: Direct Self-Assembly of Colloidal Materials. *MRS Bull.* **1998**, *23* (10), 21 (Special issue).
(6) Norris, D.; Vlasov, Y. *Adv. Mater.* **2001**, *13*, 371.
(7) Yang, P. D.; Rizvi, A. H.; Messer, B.; Chmelka, B. F.; Whitesides, G. M.; Stucky, G. D. *Adv. Mater.* **2001**, *13*, 427.
(8) Johnson, S. G.; Joannopoulos, J. D. *Acta Mater.* **2003**, *51*, 5823.
(9) Matijević, E. *Acc. Chem. Res.* **1981**, *14*, 22.
(10) Matijević, E. *Annu. Rev. Mater. Sci.* **1985**, *15*, 483.
(11) Matijević, E. *Langmuir* **1986**, *2*, 12.
(12) Sugimoto, T. *Adv. Colloid Interface Sci.* **1987**, *28*, 65.
(13) Matijević, E. *Pure Appl. Chem.* **1988**, *60*, 1479.
(14) Matijević, E. *Chem. Mater.* **1993**, *5*, 412.
(15) Matijević, E. *Langmuir* **1994**, *10*, 8.
(16) Goia, D. V.; Matijević, E. *New J. Chem.* **1998**, 1203.
(17) Xia, Y. N.; Gates, B.; Yin, Y.; Lu, Y. *Adv. Mater.* **2000**, *12*, 693.
(18) Cushing, B. L.; Kolesnichenko, V. L.; O'Connor, C. J. *Chem. Rev.* **2004**, *104*, 3893.
(19) Goia, D. V. *J. Mater. Chem.* **2004**, *14*, 451.
(20) Stöber, W.; Fink, A. *J. Colloid Interface Sci.* **1968**, *26*, 62.
(21) *Science and Technology of Polymer Colloids*; Poehlein, G. W., Ottewill, R. H., Goodwin, J. W. , Eds.; Martinus Nijhoff: Boston, MA, 1983; Vol. II.
(22) *Emulsion Plomerization*; Piirma, I., Ed.; Academic Press: New York, 1982.
(23) Shaw, W. H. R.; Bordeaux, J. J. *J. Am. Chem. Soc.* **1955**, *77*, 4729.
(24) Lamer, V. K.; Dinegar, R. H. *J. Am. Chem. Soc.* **1950**, *72*, 4847.
(25) Bogush, G. H.; Tracy, M. A.; Zukoski, C. F. *J. Non-Cryst. Solids* **1988**, *104*, 95.
(26) Calvert, P. *Nature* **1994**, *367*, 119.

10.1021/cm7033257 CCC: $40.75
Published on Web 02/20/2008

types of micrometer-sized colloidal particles might be formed via aggregation of much finer subunits rather than continuous growth by diffusion of species from the solution toward the surfaces of the nuclei. In addition, the uniformity in size for the final product might also be achieved via a self-sharpening process[12,30–40] during which, depending on the materials (the solubility product) involved and kinetic factors, either smaller particles grow faster than the bigger ones or the smaller particles vanish via Ostwald ripening because of their higher solubilities in the reaction media arising from the Gibbs–Thomson effect.[12]

Among the many types of monodispersed colloids synthesized via UBHP, the lanthanides have been studied more extensively and systematically, mainly by Matijević et al.[41–43] and Akinc and Sordelet,[44–46] owing to their interesting optical, magnetic, electrical, and catalytic properties and their wide applications in various aspects of contemporary science and technology.[47] It was demonstrated that the lanthanides generally form basic-carbonate type colloidal spheres and that the solution chemistry of the lanthanides is dependent on the ionic radius of the element,[41–46] manifesting the "lanthanide contraction phenomena".[48] Yttrium, though not a lanthanide, obeys the lanthanide contraction law and exhibits physicochemical properties close to those of holmium (Ho)[48] because of the very similar ionic radii ($r_{Dy^{3+}} = 0.0912$ nm, $r_{Y^{3+}} = 0.0900$ nm, and $r_{Ho^{3+}} = 0.0901$ nm for sixfold coordination)[49] of the two elements.

It is noteworthy that the UBHP methodology, though repeatedly successful in making monodispersed colloidal spheres of some single lanthanides, has rarely been extended to mixed lanthanide systems. For a system of mixed lanthanides, there are several issues that need to be addressed but have not been addressed well before:[43,50] (1) How does the second lanthanide affect precipitation kinetics and therefore particle morphology? (2) What is the distribution of the second lanthanide? Are the products composite particles or mechanical mixtures of two different types of particles? (3) If composite particles result, is there any concentration gradient within each particle with regard to the two lanthanides? In this paper we answered these questions through a study of the Y/Gd system, and the derived conclusions may have wide implications to other mixed systems. The Y/Gd system was chosen here for a couple of reasons: (1) the oxides (Y_2O_3/Gd_2O_3) of this system are well-known red phosphors after Eu^{3+} doping and are currently widely used in displays such as plasma display panels (PDP), field emission displays (FED), and cathode-ray tubes (CRT).[51–56] Spray pyrolysis has been able to produce spherical phosphor particles, but the resultant particles mostly have hollow structures and show wide size distributions in the nanomicrometer regime,[51,54] although a narrow size distribution is desired for uniform luminescence. Furthermore, the FED technology requires a phosphor screen to be operated under a low electron accelerating voltage of 1–5 kV. For Eu^{3+} activated $Y_2O_3-Gd_2O_3$, the electron penetration depth was estimated to be around 60 nm at an acceleration voltage of 5 kV.[52] Therefore, finer spherical particles of uniform size are desired in view of resource reservation. (2) The single oxides and the solid solutions in the Y_2O_3/Gd_2O_3 system are cubic-structured (space group: $Ia\bar{3}$) under atmospheric conditions, which makes it possible their sintering to an optically fully transparent state.[57–60] Single crystals of Y_2O_3/Gd_2O_3 are difficult to obtain in large sizes by the Czochralski method or by the floating zone technique due to their high melting points (~2430 °C for Y_2O_3 and ~2320 °C for Gd_2O_3).[61] As alternatives to single crystals, polycrystalline transparent ceramics of Y_2O_3/Gd_2O_3 may find wide applications in areas such as high-temperature windows, solid lasers,[61] and ceramic scintillators (after activator doping).[59] The fabrication of transparent ceramics similarly needs dispersed spherical particles of a sharp size distribution to allow a uniform packing of the particles in the green body and a uniform densification of the green body upon sintering.[62–64]

(27) Ocaña, M.; Rodriguez-Clemente, R.; Serna, C. J. *Adv. Mater.* **1995**, *7*, 212.
(28) Privman, V.; Goia, D. V.; Park, J.; Matijević, E. *J. Colloid Interface Sci.* **1999**, *213*, 36.
(29) Park, J.; Privman, V.; Matijević, E. *J. Phys. Chem. B* **2001**, *105*, 11630.
(30) Overbeek, J. T. G. *Adv. Colloid Interface Sci.* **1982**, *15*, 251.
(31) Flagan, R. C. *Ceram. Trans.* **1988**, *1* (A), 229.
(32) Look, J.-L.; Bogush, G. H.; Zukoski, C. F. *Faraday Discuss.* **1990**, *90*, 345.
(33) Dirksen, J. A.; Benjelloun, S.; Ring, T. A. *Colloid Polym. Sci.* **1990**, *268*, 864.
(34) Bogush, G. H.; Zukoski, C. F. *J. Colloid Interface Sci.* **1991**, *142*, 19.
(35) Brilliantov, N. V.; Krapivsky, P. L. *J. Phys. A* **1991**, *24*, 4787.
(36) Dirksen, J. A.; Ring, T. A. *Chem. Eng. Sci.* **1991**, *46*, 2389.
(37) Ring, T. A. *Powder Technol.* **1991**, *65*, 195.
(38) Van Blaaderen, A.; van Geest, J.; Vrij, A. *J. Colloid Interface Sci.* **1992**, *154*, 481.
(39) Ludwig, F.-P.; Schmelzer, J. J. *Colloid Interface Sci.* **1996**, *181*, 503.
(40) Lee, K.; Look, J.-L.; Harris, M. T.; McCormick, A. V. *J. Colloid Interface Sci.* **1997**, *194*, 78.
(41) Matijević, E.; Hsu, W. P. *J. Colloid Interface Sci.* **1987**, *118*, 506.
(42) Hsu, W. P.; Rönnquist, L.; Matijević, E. *Langmuir* **1988**, *4*, 31.
(43) Aiken, B.; Hsu, W. P.; Matijević, E. *J. Am. Ceram. Soc.* **1988**, *71*, 845.
(44) Akinc, M.; Sordelet, D. *Adv. Ceram. Mater.* **1987**, *2*, 232.
(45) Sordelet, D.; Akinc, M. *J. Colloid Interface Sci.* **1988**, *122*, 47.
(46) Akinc, M. In *Fourth Euro Ceramics*; Galassi, C., Ed.; Gruppo Editoriale Faenza Editrice: Faenza, 1995; Vol. 1.
(47) *Industrial Applications of Rare Earth Elements*; Gschneider, K. A., Jr., Ed.; American Chemical Society: Washington, DC, 1981..
(48) Sidgwick, N. V. *Chemical Elements and Their Compounds*; Clarendon Press: Oxford, 1962, Vol. 1.
(49) Shannon, R. D. *Acta Crystallogr.* **1976**, *A32*, 751.
(50) Li, J.-G.; Ikegami, T.; Wang, Y.; Mori, T. *J. Am. Ceram. Soc.* **2003**, *86*, 915.
(51) Kang, Y. C.; Roh, H. S.; Park, S. B. *Adv. Mater.* **2000**, *12*, 451.
(52) Wakefield, G.; Holland, E.; Dobson, P. J.; Hutchison, J. L. *Adv. Mater.* **2001**, *13*, 1557.
(53) Byeon, S.-H.; Ko, M.-G.; Park, J.-C.; Kim, D.-K. *Chem. Mater.* **2002**, *14*, 603.
(54) Kim, E. J.; Kang, Y. C.; Park, H. D.; Ryu, S. K. *Mater. Res. Bull.* **2003**, *38*, 515.
(55) Sun, L.; Liao, C.; Yan, C. J. *Solid State Chem.* **2003**, *171*, 304.
(56) Lenggoro, I. W.; Itoh, Y.; Okuyama, K. *J. Mater. Res.* **2004**, *19*, 3534.
(57) Rhodes, W. H. *J. Am. Ceram. Soc.* **1981**, *64*, 13.
(58) Greskovich, C.; O'Clair, C. R. *Adv. Ceram. Mater.* **1986**, *1*, 350.
(59) Greskovich, C. D.; Cusano, D.; Hoffman, D.; Riedner, R. J. *Am. Ceram. Soc. Bull.* **1992**, *71*, 1120.
(60) Ikegami, T.; Li, J.-G.; Mori, T.; Moriyoshi, Y. *J. Am. Ceram. Soc.* **2002**, *85*, 1725.
(61) Fornasiero, L.; Mix, E.; Peters, V.; Petermann, K.; Huber, G. *Ceram. Int.* **2000**, *26*, 589.
(62) Lange, F. F. *J. Am. Ceram. Soc.* **1989**, *72*, 3.
(63) Li, J.-G.; Ikegami, T.; Lee, J.-H.; Mori, T.; Yajima, Y. *J. Eur. Ceram. Soc.* **2000**, *20*, 2395.
(64) Rhodes, W. H.; Trickett, E. A.; Sordelet, D. J. In *Ceramic Transactions: Ceramic Powder Science III*; Messing, G. L., Fuller, E. R., Hausner, H., Eds.; The American Ceramic Society, Inc.: Westerville, OH, 1988.

2. Experimental Section

2.1. Particle Preparation. In a typical synthetic procedure for colloidal precursor particles, proper amounts of $Y(NO_3)_3 \cdot 6H_2O$ (>99.99% pure), $Gd(NO_3)_3 \cdot 6H_2O$ (>99.95% pure), and urea ($CO(NH_2)_2$, >99% pure) were dissolved in distilled water to make a total volume of 2000 mL. All the chemicals were supplied by Kanto Chemical Co., Inc., Tokyo, Japan, and were used as received. In all the cases, the total concentration of Gd^{3+} and Y^{3+} was kept constant at 0.015 M while that of urea was kept at 0.5 M. The Gd^{3+} to total cation molar ratio R was varied ($R = Gd^{3+}/(Y^{3+} + Gd^{3+}) = 0$, 0.1, 0.2, 0.25, 0.3, 0.4, 0.5, 0.75, and 1.0) to investigate its effects on precipitation kinetics and particle morphology. The mixed solution, contained in a beaker wrapped with aluminum foil, was first homogenized under magnetic stirring at room temperature for 2 h and was then heated on a hot plate to 90 ± 1 °C within 60 min. After reacting at 90 ± 1 °C for 2 h, the suspension was cooled naturally to ~50 °C, and the resultant colloidal particles were recovered via suction filtration through a 0.2 micron membrane. Byproducts of the reaction were removed by washing the particles with distilled water via ultrasonication and suction filtration four times. After rinsing with anhydrous ethanol (except the part for elemental analysis), the particles were dried in an air oven at 100 °C for 24 h and were then calcined in a tube furnace under flowing O_2 gas (100 mL/min) to produce oxide particles. To understand the precipitation mechanism, 30 mL of the colloidal suspension was sampled regularly since visible turbidity appeared in the originally clear solution. The sampled suspension was quenched with iced water and was centrifuged to achieve solid/liquid separation. After washing and drying as described above, the particles were used for further analysis.

2.2. Characterization Techniques. Compositions of the precursor particles were determined by elemental analysis. The Y^{3+} and Gd^{3+} contents were analyzed by the inductively coupled plasma (ICP) spectrophotometric method with an accuracy of 0.01 wt %; carbon content was assayed on a simultaneous carbon/sulfur determinator with a detection limit of 0.01 wt % (model CS-444LS, LECO, St. Joseph, MI, USA); and NH_4^+ content was determined by the standard distillation-titrimetric method with an experimental error of ±0.1 wt %.

Morphologies of the particles were observed via field-emission scanning electron microscopy (FE-SEM, model S-5000, Hitachi, Tokyo). Average diameter and standard size deviation of the particles were derived from 200 randomly selected particles with an image analysis software.

Thermogravimetry (TG, model TAS-200, Rigaku, Tokyo) of the dried precursor particles was made under flowing air (100 mL/min) with a heating rate of 10 °C/min.

Phase identification was performed via X-ray diffractometry (XRD) on a Philips PW1800 X-ray diffractometer (Philips Research Laboratories, Eindhoven, The Netherlands) operating at 40 kV/50 mA using nickel-filtered Cu Kα radiation in the range of 2θ = 10−70 ° with a scanning speed of 0.15° 2θ per minute. Lattice parameters of the oxides were determined by fitting the observed reflections with a least-squares refinement program.

Optical properties of the $(Y_{1-x}Gd_x)_2O_3$ solid-solution oxides were studied via UV–vis absorption spectroscopy (model V-570, JASCO Co., Tokyo).

3. Results and Discussion

3.1. Synthesis, Characterization, and Formation Mechanism of the Colloidal Precursor Spheres. Elemental contents and chemical formulas of the dried colloidal particles are summarized in Table 1, from which it was concluded that quantitative precipitation of Y and Gd was achieved for the mixed systems after 2 h of reaction at 90 ± 1 °C and that the products all have an approximate chemical composition of $(Y,Gd)(OH)CO_3 \cdot 1.3H_2O$. NH_4^+ was analyzed in each case, but its content was found to be below the detection limit (0.1 wt %) of the analysis method. All the dried particles are amorphous to X-rays. The formation of amorphous basic-carbonate particles via UBHP conforms to previous reports.[41–46,50] Chemical analysis of the supernatant after removal of solid particles shows that the remnant concentrations of Y and Gd are both below the detection limit of 0.01 wt % after 2 h of reaction at 90 ± 1 °C, indicating an almost complete precipitation.

Table 1. Elemental Contents and Chemical Formulas of the Colloidal Particles

intended Gd content (atom %)	Y (wt %)	Gd (wt %)	C (wt %)	formula
0	46.96	0	6.33	$Y(OH)CO_3 \cdot 1.3H_2O$
10	40.72	8.00	6.10	$(Y_{0.9}Gd_{0.1})(OH)CO_3 \cdot 1.32H_2O$
20	35.16	15.55	5.91	$(Y_{0.8}Gd_{0.2})(OH)CO_3 \cdot 1.26H_2O$
25	32.30	19.05	5.80	$(Y_{0.75}\ Gd_{0.25})(OH)CO_3 \cdot 1.3H_2O$
30	29.69	22.48	5.72	$(Y_{0.7}Gd_{0.3})(OH)CO_3 \cdot 1.3H_2O$
40	24.53	28.92	5.52	$(Y_{0.6}Gd_{0.4})(OH)CO_3 \cdot 1.35H_2O$
50	20.23	35.72	5.44	$(Y_{0.5}Gd_{0.5})(OH)CO_3 \cdot 1.1H_2O$
75	9.26	49.14	5.1	$(Y_{0.25}Gd_{0.75})(OH)CO_3 \cdot 1.27H_2O$
100	0	61.05	4.63	$Gd(OH)CO_3 \cdot 1.3H_2O$

Figure 1 shows morphologies of the resultant colloidal particles (redispersed from dried powders) for some typical compositions. It can be seen that monodispersed colloidal spheres are obtainable with the UBHP methodology for mixed Y/Gd systems and that a higher Gd content steadily leads to finer particles. As the colloidal spheres of pure Y and Gd systems exhibit distinctly different sizes (Figure 1a,f), the uniform particle diameter observed for each Y/Gd mixed system may thus imply that the particles are solid solutions

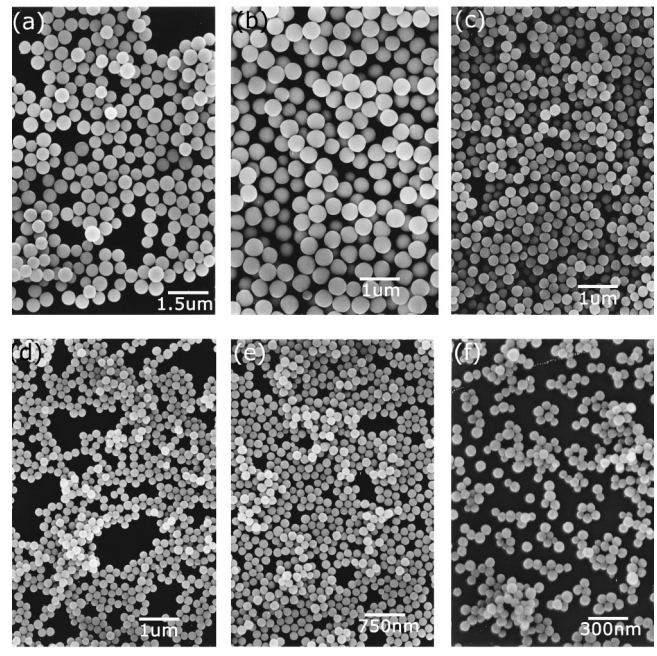

Figure 1. FE-SEM micrographs showing morphologies of the resultant colloidal particles for some typical compositions, with $R = 0$ (a), $R = 0.1$ (b), $R = 0.3$ (c), $R = 0.5$ (d), $R = 0.75$ (e), and $R = 1.0$ (f).

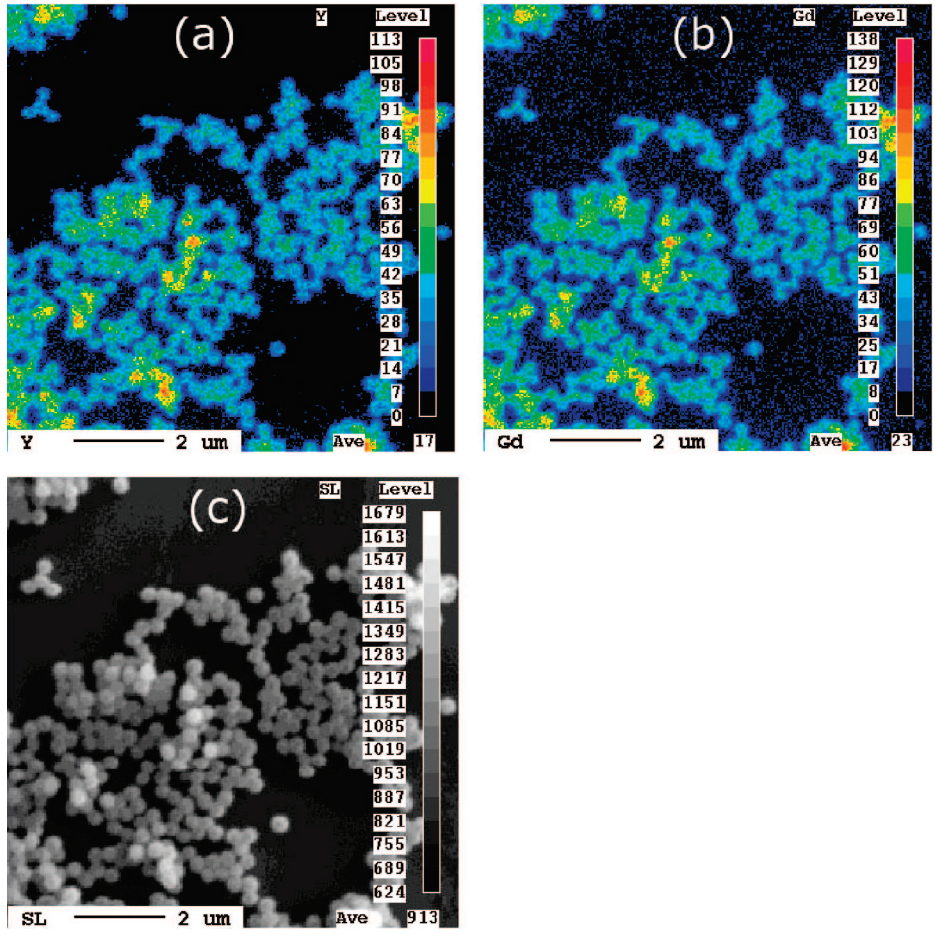

Figure 2. Elemental mapping of the colloidal precursor spheres with a composition of $R = 0.2$, with (a) the distribution of Y, (b) the distribution of Gd, and (c) the SEM particle morphology.

rather than mechanical mixtures of $Y(OH)CO_3$ and $Gd(OH)CO_3$. Elemental mapping of Y and Gd provides direct evidence of the solid−solution nature of the particles, as shown in Figure 2 for the $R = 0.2$ composition. It was observed that each particle contains both Y and Gd and that the two elements are quite evenly distributed among the particles.

As the colloidal spheres are formed via nucleation/growth processes, the decreased average size at a higher Gd content thus suggests increased nucleation density by Gd addition. The key to any chemical precipitation is the degree of supersaturation, S, given by

$$S = a_A a_B / K_{sp} \tag{1}$$

where a_A and a_B are the activities of the partially hydrolyzed cation ($[Ln(OH)_x(H_2O)_y]^{3-x}$, $x + y = 6$, Ln = Y, Gd)[41] and anion (CO_3^{2-}), respectively, and K_{sp} is the solubility product constant. Nucleation starts only when S reaches the critical supersaturation S^*. The lanthanide contraction phenomena predict a higher solubility (larger K_{sp}) of $Y(OH)CO_3$ than $Gd(OH)CO_3$ in water,[65,66] from which it can be inferred that the S value is smaller for $Y(OH)CO_3$ and hence stable nuclei of $Y(OH)CO_3$ are relatively difficult to form.

Meanwhile, the homogeneous nucleation rate, R_N, can be correlated to S via the equation[18]

$$R_N = A \exp\left(\frac{-16\pi\sigma_{SL}v^2}{3k^3T^3 \ln^2 S}\right) \tag{2}$$

where R_N is the number of nuclei formed per unit time per unit volume, A is a pre-exponential constant typically ranging from 10^{25} to 10^{56}, σ_{SL} is the surface tension at the liquid/solid interface, v is the atomic volume of the solute, k is the Boltzmann constant, and T is temperature. Equation 2 may then suggest a lower nucleation rate for the pure Y system due to its smaller S value. As the cation and urea concentrations have been kept constant throughout this investigation, it is thus understandable that the resultant $Y(OH)CO_3$ has a bigger average particle diameter, through more growth, than $Gd(OH)CO_3$. For mixed Y/Gd systems, the nucleation of $Gd(OH)CO_3$ occurs in priority, and the precipitation of $Y(OH)CO_3$ may largely take place via heterogeneous nucleation on the already formed $Gd(OH)CO_3$ nuclei. The higher the Gd content, the higher the nucleation density and thus the smaller the average sizes of the resultant colloidal particles.

Plotting the mean particle diameter against the Gd content revealed two regions of linear relationships divided at $R =$

(65) Krumholz, P. In *Solution Chemistry, in Progress in the Science and Technology of the Rare Earths*; Eyring, L., Ed.; Pergamon Press: New York, 1964.

(66) Ryabchikov, D. I.; Terentyeva, E. A. In *Recent Soviet Research on the Chemistry of Rare Earth Complexes, in Progress in the Science and Technology of the Rare Earths*; Eyring, L., Ed.; Pergamon Press: New York, 1964.

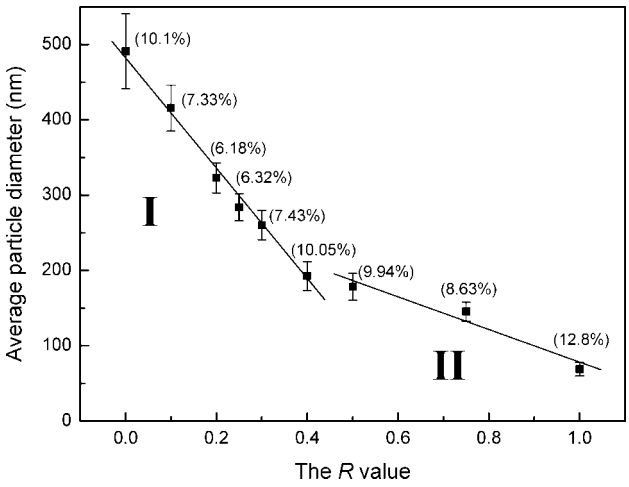

Figure 3. Average diameter of the colloidal particles as a function of the Gd content. The standard size deviations in nanometers are given out as error bars while the figure in brackets at each data point denotes the deviation in percentage.

0.5, that is, $Y^{3+}/Gd^{3+} = 1{:}1$ molar ratio (Figure 3). Such linear relationships indicate that the average particle size is inversely proportional to nucleation density. The changed slopes of the two linear lines are a direct manifestation of the altered predominance of the constituent elements. When Gd becomes the major component ($R \geq 0.5$, Region II), the whole precipitation process is dominated by the nucleation and growth of $Gd(OH)CO_3$ and therefore the influences of Y become weaker, yielding a less steep slope.

Growth kinetics of the colloidal spheres was monitored continuously for 30 min since visible turbidity appeared in the originally transparent solution. Figure 4 shows morphologies of the regularly sampled colloidal particles, with the $R = 0.3$ composition as an example, from which a quite uniform growth was observed. The evolution of particle diameter with reaction time is presented in Figure 5a for some typical compositions. Clearly, the growth rate is dependent upon the Gd content. This is another manifestation of the increased nucleation density by Gd addition. As the total concentration of Gd^{3+} and Y^{3+} has been kept constant in each case, the more the nuclei formed, the fewer the solutes left behind for particle growth and thus the less the growth. The particle growth data (Figure 5a) can be fitted well with the cubic-root law (Figure 5b) given by $D(t) = (Kt)^{1/3}$, where $D(t)$ is the average particle diameter at time t, K is the growth rate, and t is reaction time. This implies that the growth is a diffusion-controlled process.[18] The K values determined from Figure 5b for compositions of $R = 0$, 0.3, 0.5, and 0.75 are $\sim 2.69 \times 10^6$, 7.54×10^4, 4.07×10^4, and 2.12×10^4 nm^3/min, respectively, further revealing the pronounced impacts of Gd content on nucleation and growth.

While the above-mentioned differential nucleation explains well the observed Gd effects on particle size and particle growth, there must be concentration gradients within each particle with regard to Y and Gd should it actually occur. Composition evolution of the colloidal spheres has been investigated through elemental analysis via ICP of their instantaneous cation contents, with the $R = 0.3$ sample as an example. The relative content of Gd in the particles can

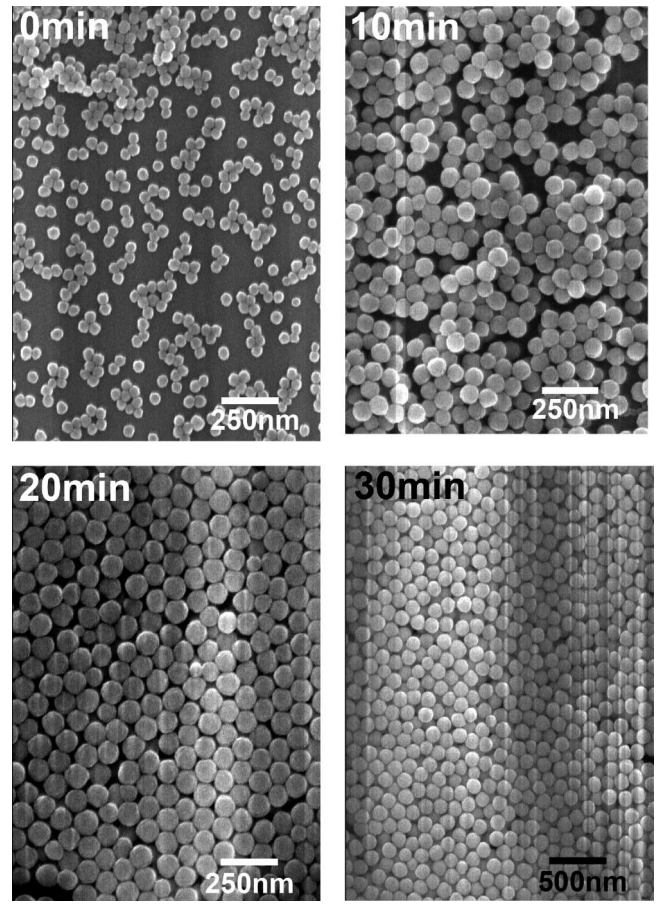

Figure 4. FE-SEM micrographs showing morphologies of the colloidal particles ($R = 0.3$) during growth. "0 min" denotes the starting point of analysis at which visible turbidity appears in the originally clear solution.

be expressed as a Gd/(Y + Gd) molar ratio or 1/(1 + Y/Gd), and the value should remain constant at 0.3 (the intended Y/Gd molar ratio is 7/3) during the whole process of reaction should stoichiometric precipitation take place instantaneously for Y and Gd. A hyper-stoichiometric precipitation of Gd leads to a smaller Y/Gd ratio and hence a higher Gd/(Y + Gd) value. The results of the elemental analysis are presented in Figure 6. Indeed, along with particle growth, more Y was built in, or in other words the final resultant particles have increased Gd content going from surfaces to cores. It can also be inferred from Figure 6 that complete precipitation was achieved after 75 min of reaction at 90 ± 1 °C, and then the particles turn overall stoichiometric.

The conclusions drawn from this part of the study may have wide implications to other mixed systems when employing the UBHP technique for their synthesis. For example, doping the Y_2O_3/Gd_2O_3 system with activator ions (such as Nd^{3+}, Tb^{3+}, Eu^{3+}, etc.) is indispensable for optical applications. In such cases, adequate annealing would be necessary to obtain high luminous efficiencies, through eliminating the concentration gradient (localized concentration quenching of luminescence) induced by differential nucleation. We actually observed that Eu^{3+} ions have more pronounced effects than Gd^{3+} on nucleation/growth and the composition gradient, owing to its even larger ionic size (0.0947 nm for sixfold coordination)[49] and the even smaller

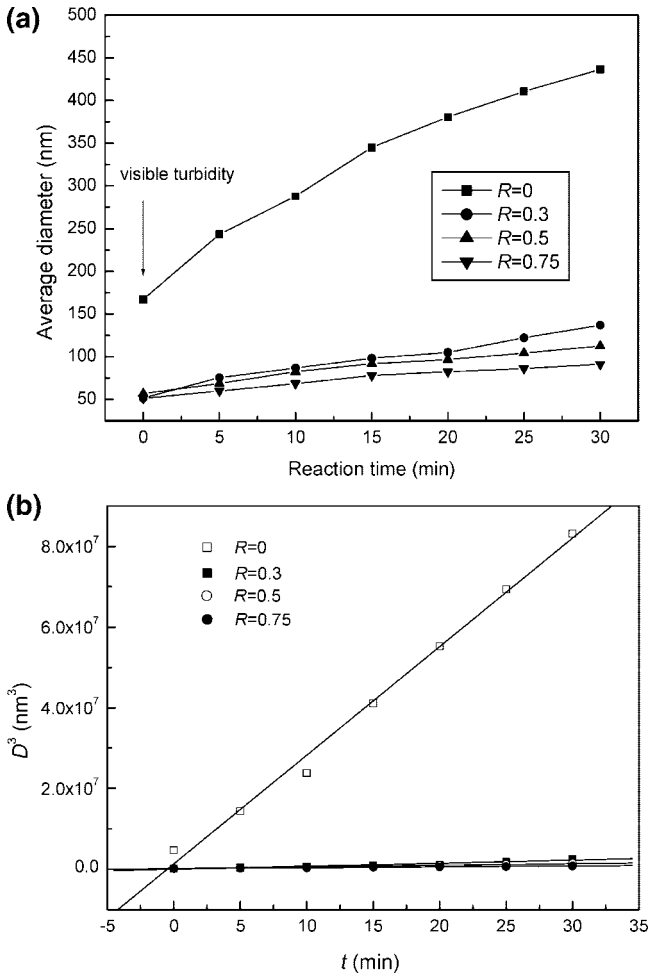

Figure 5. Size evolution of the colloidal spheres for some typical compositions (a), and fitting the growth data according to the cubic-root law (b).

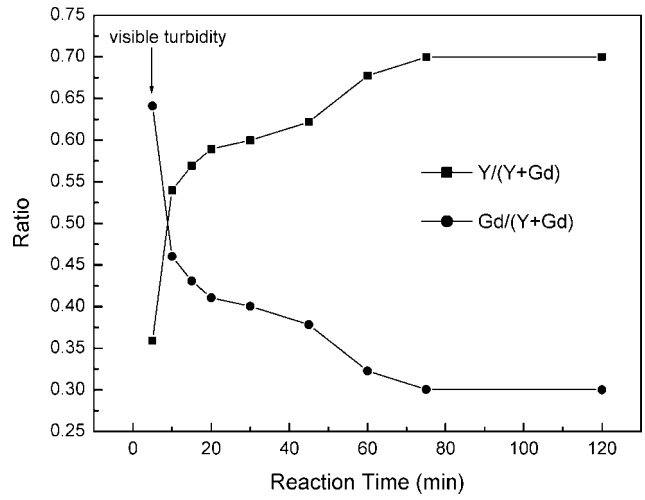

Figure 6. Composition evolution of the colloidal particles for the $R = 0.3$ composition.

solubility product of $Eu(OH)CO_3$. Kawahara et al.[67] recently made submicrometer-sized $Y_2O_2S:Eu^{3+}$ phosphor particles via sulfurizing the precursors synthesized via complex homogeneous precipitation in the presence of urea, and they

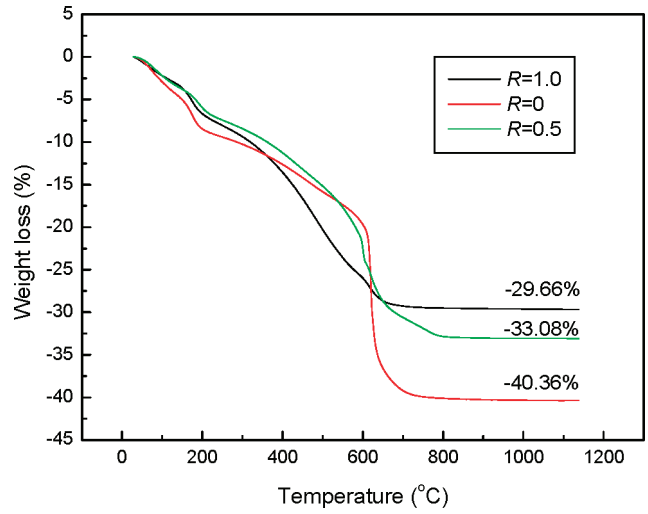

Figure 7. Decomposition behaviors of the dried colloidal particles for three typical compositions.

claimed that the observed excellent luminous intensity after annealing the particles at relatively high temperatures is due to the decreased defect concentration and so on. Another important reason, however, must have been missed there: the diminished concentration gradient of Eu^{3+} at higher temperatures. Detailed characterizations of our Eu^{3+}-doped samples are now underway.

3.2. Properties of the Derived Oxides. Figure 7 exhibits decomposition behaviors of the basic carbonate particles for three typical compositions. Complete conversions to oxides occur up to ~800 °C, and the observed weight losses are close to the values calculated from the corresponding chemical formulas (40.4 wt % for $Y(OH)CO_3 \cdot 1.3H_2O$, 29.6 wt % for $Gd(OH)CO_3 \cdot 1.3H_2O$, and 33.1 wt % for $(Y_{0.5}Gd_{0.5})(OH)CO_3 \cdot 1.1H_2O$).

Figure 8 shows morphologies of the oxide particles calcined up to 1000 °C for some typical compositions. The spherical shape and good dispersion of the precursor particles is retained in the oxides for all the compositions except pure Gd_2O_3, which, due to its finest average size of the precursor particles, exhibits partial sintering (neck formation among adjacent spheres) at 850 °C and irregular morphologies after significant coarsening at an even higher temperature of 1000 °C. Eu^{3+} activated Y_2O_3/Gd_2O_3 particles are known to exhibit sharp red luminescence, typically at ~610 nm arising from the $^5D_0 \rightarrow {}^7F_2$ electronic transition of the Eu^{3+} ions, upon excitation into the charge transfer (CT) band at ~254 nm. The luminescence behavior and luminescence uniformity are dependent upon particle size and size distribution, as smaller particles tend to have more surface states than bigger ones.[68] The uniform morphology obtained with this UBHP technique may allow a homogeneous distribution of Eu^{3+} among the particles and thus a highly uniform luminescence.

Figure 9 demonstrates XRD patterns of the oxides obtained at 1000 °C for five representatives. No other phase was identified along with the cubic structured $(Y_{1-x}Gd_x)_2O_3$ (x = 0–1), though monoclinic structured Gd_2O_3 and $(Y_{1-x}Gd_x)_2O_3$ solid solutions were reported to form in the powders processed

(67) Kawahara, Y.; Petrykin, V.; Ichihara, T.; Kijima, N.; Kakihana, M. *Chem. Mater.* **2006**, *18*, 6303.

(68) Wu, C.; Qin, W.; Qin, G.; Zhao, D.; Zhang, J.; Huang, S.; Lü, S.; Liu, H.; Lin, H. *Appl. Phys. Lett.* **2003**, *82*, 520.

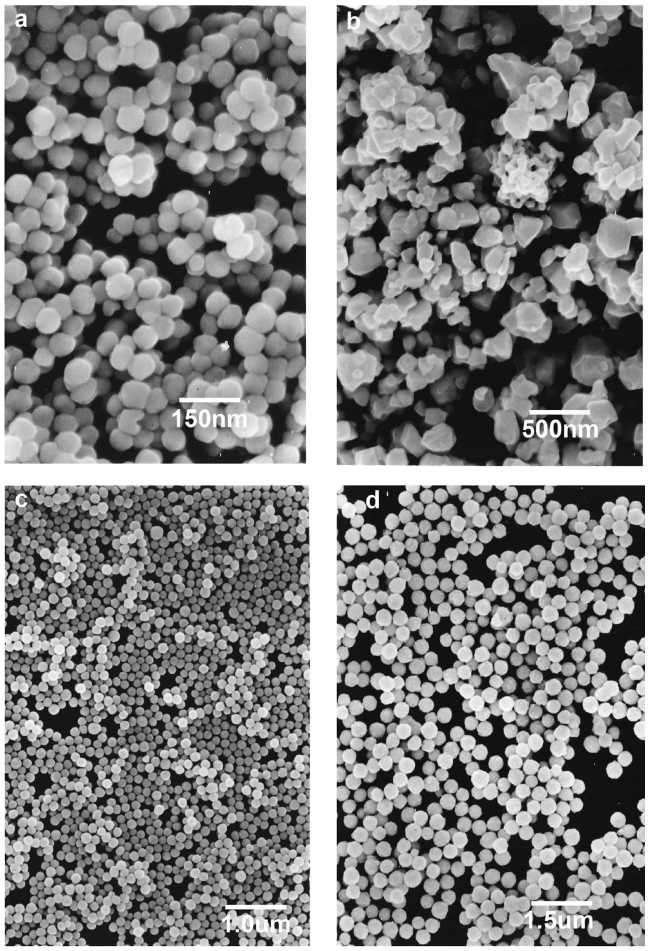

Figure 8. FE-SEM micrographs showing morphologies of the oxide particles obtained by calcining the dried colloidal particles, with (a) the $R = 1.0$ sample at 850 °C, (b) the $R = 1.0$ sample at 1000 °C, (c) the $R = 0.5$ sample at 1000 °C, and (d) the $R = 0$ sample at 1000 °C.

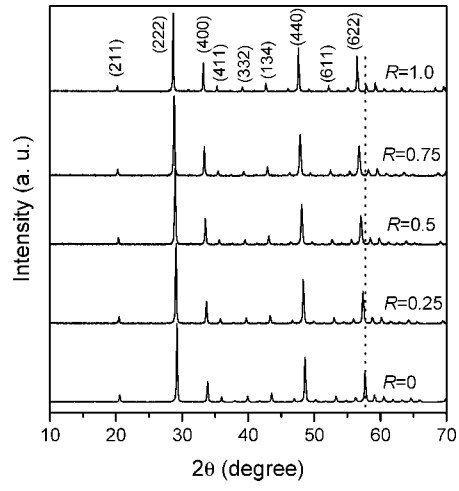

Figure 9. Typical XRD patterns of the oxides calcined at 1000 °C.

via gel combustion.[55] The XRD peaks steadily shift toward the low angle side along with increased Gd addition, indicating a gradually expanded unit cell of the crystal structure. This is due to the larger ionic radius of Gd^{3+} (0.0938 nm for sixfold coordination) than that (0.0900 nm for sixfold coordination) of Y^{3+}.[49] The lattice constants determined from the XRD patterns are $a = 10.610 \pm 0.003$ Å for Y_2O_3 and $a = 10.817 \pm 0.005$ Å for Gd_2O_3, which

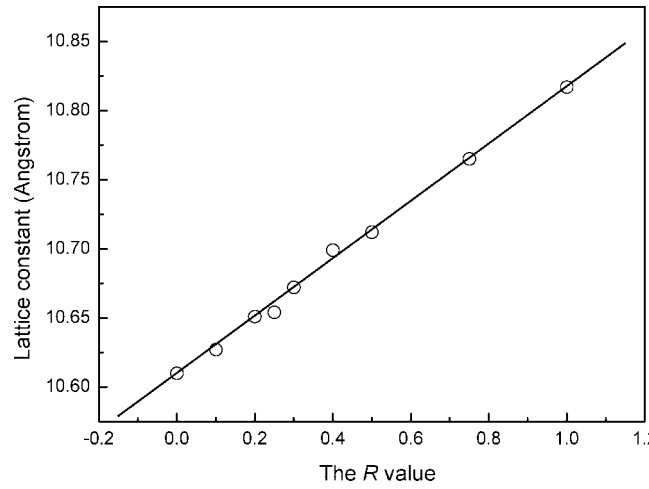

Figure 10. Lattice parameters of the oxides calcined at 1000 °C, as a function of the Gd content.

are slightly larger but close to the reported values (JCPDS, 43-1036, $a = 10.604$ Å for Y_2O_3; JCPDS, 43-1014: $a = 10.813$ Å for Gd_2O_3). Figure 10 exhibits lattice constants of the oxides pyrolyzed at 1000 °C for the full range of compositions studied in this work. Clearly, the cell parameter observes the Vegard's law and shows linear dependence on the Gd content, which suggests that, though concentration gradients exist within each precursor sphere, 1000 °C has been high enough for the formation of continuous solid solutions between Y_2O_3 and Gd_2O_3.

Optical properties of the oxides obtained at 1000 °C were studied with UV–vis absorption spectroscopy, and the results are presented in Figure 11a for some representatives. Apparently Gd enhances UV absorption and red-shifts the absorption edge. In addition, the $^8S_{7/2} \rightarrow {}^6I_J$ transitions of Gd^{3+} ions[69,70] were observed at 276 nm for pure Gd_2O_3 and the solid solutions. Estimations of bandgap energies can be made from the absorption spectra. The relation between absorption coefficient (α) and incident photon energy ($h\nu$) can be written as $\alpha = B_d(h\nu - E_g)^{1/2}$, where B_d is the absorption constant while E_g is the bandgap energy.[71] Plots of $(Ah\nu)^2$ versus $h\nu$ from the spectral data of Figure 11a are presented in Figure 11b. Extrapolating the linear parts of the curves for pure Y_2O_3 and Gd_2O_3 yields bandgap values of 5.57 and 5.20 eV, which are in close vicinity to those of 5.50 and 5.20 eV experimentally determined for single crystals of Y_2O_3[72] and Gd_2O_3,[73] respectively. Bandgaps of the solid solutions fall between those of the single oxides (Figure 11b). Figure 12 shows bandgaps of the oxides for all the compositions investigated in this work. It can be seen that the bandgap decreases linearly along with increased Gd content. This may provide another evidence that continuous solid solutions are directly formed by heating the precursor particles at 1000 °C. In addition, the enhanced UV absorption

(69) Li, Y.; Hong, G. *J. Lumin.* **2007**, *124*, 297.
(70) Li, Y.-C.; Chang, Y.-H.; Chang, Y.-S.; Lin, Y.-J.; Laing, C.-H. *J. Phys. Chem. C* **2007**, *111*, 10682.
(71) Hagfeldt, A.; Gratzel, M. *Chem. Rev.* **1995**, *95*, 49.
(72) Tomiki, T.; Tamashiro, J.; Tanahara, Y.; Yamada, A.; Fukutani, H.; Miyahara, T.; Kato, H.; Shin, S.; Ishigame, M. *J. Phys. Soc. Jpn.* **1986**, *55*, 4543.
(73) Jia, D.; Lu, L.; Yen, W. M. *Opt. Commun.* **2002**, *212*, 97.

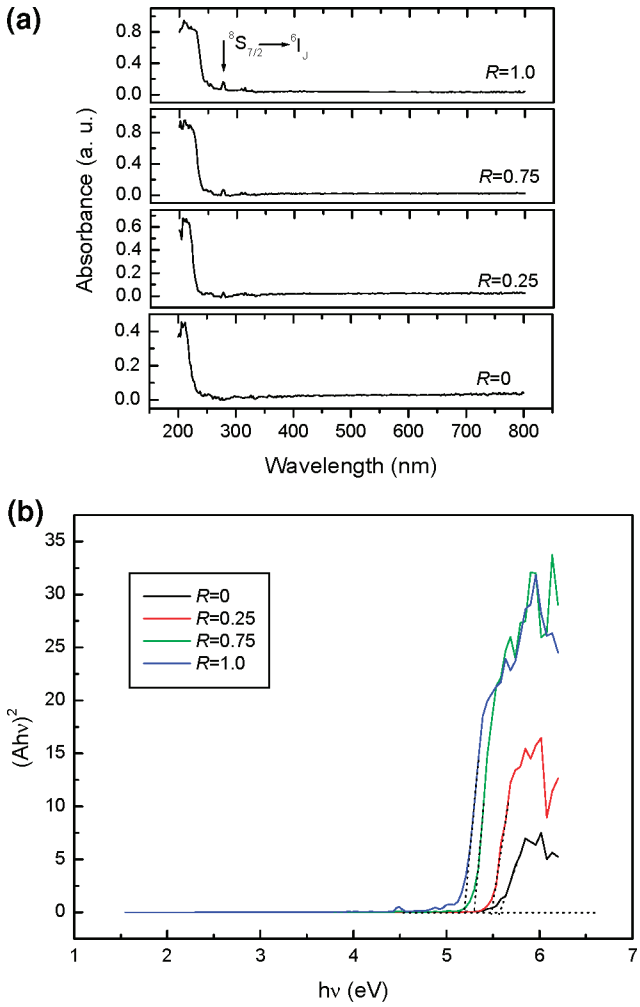

Figure 11. UV–vis absorption spectra (a) and the determination of bandgap energies (b) for some typical oxides obtained at 1000 °C. *A* in the *Y* axis title of part (b) represents absorbance, which is proportional to the absorption coefficient α.

(Figure 11a) and the decreased bandgap (Figure 12) by Gd addition may predict significant influences of the Gd content on luminescent properties of the activator-doped Y_2O_3/Gd_2O_3 systems in optical applications.

4. Conclusions

The UBHP technique was employed in this work to prepare basic-carbonate colloidal spheres of mixed Y/Gd systems, and properties of the resultant $(Y_{1-x}Gd_x)_2O_3$ (x = 0–1) spheres were investigated. The main conclusions are summarized as follows:

(1) The UBHP methodology is successful in making colloidal spheres of Y/Gd mixed systems, and the particles

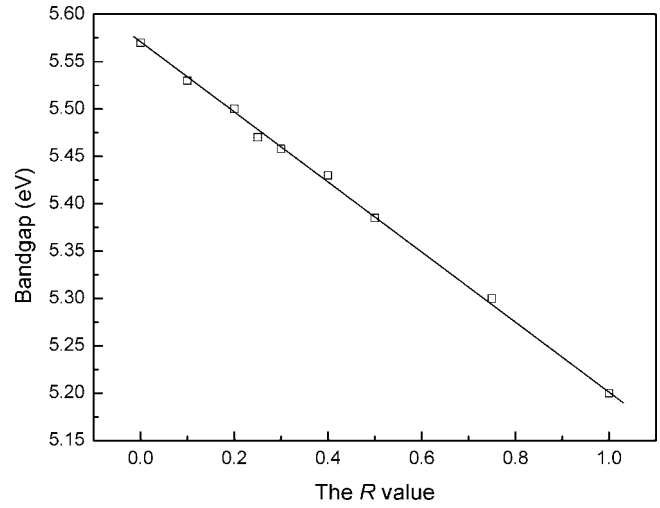

Figure 12. Bandgap energies of the oxides calcined at 1000 °C, as a function of the Gd content.

are basic carbonates having an approximate chemical composition of $(Y_{1-x}Gd_x)(OH)CO_3 \cdot 1.3H_2O$.

(2) The addition of Gd increases nucleation density and thus steadily decreases average size of the colloidal spheres. The colloidal spheres of mixed Y/Gd systems have concentration gradients with regard to Y and Gd within each particle, and the inner layer of the particle has more Gd. These phenomena are due to differential nucleation of $Y(OH)CO_3$ and $Gd(OH)CO_3$. Growth of the colloidal spheres follows the cubic-root law (diffusion controlled).

(3) The dried colloidal spheres directly convert to cubic structured $(Y_{1-x}Gd_x)_2O_3$ (x = 0–1) solid solutions at 1000 °C while largely retaining their morphologies. Both the lattice constants and the bandgaps of the oxides exhibit linear dependence on the Gd content, with the former increasing from $a = 10.610 \pm 0.003$ Å for Y_2O_3 to $a = 10.817 \pm 0.005$ Å for Gd_2O_3 while the latter decreasing from 5.57 eV for Y_2O_3 to 5.20 eV for Gd_2O_3.

Acknowledgment. Special thanks are due to Mr. Y. Yajima of Materials Analysis Station, National Institute for Materials Science (NIMS), for performing elemental analysis, Mr. K. Kosuda of Materials Analysis Station, NIMS, for elemental mapping, and Mr. M. Ikeda of Nano Ceramics Center, NIMS, for particle size analysis. This work was partially supported by Program for New Century Excellent Talents in University (NCET-25-0290), the National Science Fund for Distinguished Young Scholars (50425413), and the National Natural Science Foundation of China (50672014, 50772020).

CM7033257